J. Cent. South Univ. (2015) 22: 3536−3543
DOI: 10.1007/s11771-015-2893-z

Springer

Influences of anisotropy and inhomogeneity on supporting pressure of tunnel face with kinematical approach

YANG Xiao-li(杨小礼)[1], LI Wen-tao(李闻韬)[1], PAN Qiu-jing(潘秋景)[2]

1. School of Civil Engineering, Central South University, Changsha 410075, China;
2. Laboratory 3SR, Grenoble Alpes University, CNRS UMR 5521, Grenoble, France

Abstract: Based on the active failure mechanism generated by a spatial discretization technique, the stability of tunnel face was studied. With the help of the spatial discretization technique, not only the anisotropy and inhomogeneity of the cohesion but also the inhomogeneity of the internal friction angle was taken into account in the analysis of the supporting forces. From the perspective of upper bound theorem, the upper bound solutions of supporting pressure were derived. The influence of the anisotropy and heterogeneity on the supporting forces as well as the failure mechanisms was discussed. The results show that the spatial discretization characteristics of cohesion and internal frictional angle impose a significant effect on the supporting pressure, which indicates that above factors should be considered in the actual engineering.

Key words: tunnel face; supporting forces; anisotropy; inhomogeneity; upper bound theorem

1 Introduction

In the process of tunnel excavation, the original equilibrium of the soils in front of the tunneling face is disrupted due to stress release, thus the tunnel face is inclined to collapse. In this case, the priority should be given to maintaining the stability of the tunnel face so as to ensure the safety of tunnel construction. However, it is a rather complicated engineering issue since the instability of tunnel face has something to do with surrounding rock classification, the construction size of tunnel face, burial depth, underground water pressure, and so forth. In order to evaluate the face stability with limit analysis method, it is of great significance to throw light upon the failure mechanism which draws the outline of actual failure under the limit state, and this approach is indeed analyzed by numerous scholars worldwide.

With respect to the face stability of tunnels, diverse collapse mechanisms have been utilized by many investigators based on the assumption of isotropic and homogeneous geotechnical materials. Based on generalized Hoek-Brown strength criterion, pseudo-static analysis of face stability of a shield-driven tunnel was investigated in the presence of surface loads by constituting an active failure mode in the framework of plasticity theory [1]. In Ref. [2], multi-block failure mechanism was proposed according to the gradual velocity field of collapsing blocks in front of tunnel face during excavation. In light of this thought, the objective function of supporting pressure exerted on the tunnel face was obtained with upper bound theorem, and the corresponding optimal solutions were calculated by programming. Furthermore, the effect of relevant parameters on the supporting pressure and failure shape was discussed.

In reality, the real geotechnical materials present characteristics of anisotropy and heterogeneity due to obvious bedding structure resulting from natural sedimentary and geological tectonism, thus these factors should not be ignored in the theoretical analysis because of the significant effect on mechanical properties of geomaterials, which exerts an adverse influence on the stability of geotechnical structures such as slopes, foundations, retaining walls, and tunnels. As for research of this respect, although some authors [3−11] have studied the foundation bearing capacity in the case of a soil with an anisotropic and inhomogeneous cohesion, they did not take the anisotropic and inhomogeneous nature of the internal friction angle into account. Apart from above research, few materials involved with anisotropy and heterogeneity can be found so far.

Anisotropy and heterogeneity properties of

Foundation item: Project(2013CB036004) supported by the National Basic Research Program of China; Projects(51178468, 51378510) supported by the National Natural Science Foundation of China
Received date: 2014−10−20; **Accepted date:** 2015−06−05
Corresponding author: YANG Xiao-li; Professor; Tel: +86−14789933669, E-mail: yangky@aliyun.com

geomaterials have a dramatic impact on the face stability of tunnels to some extent and some scholars have made some researches in this respect. MOLLON et al [12] concluded that the effect of internal fractional angle change on the tunnel stability is far more than that of cohesion. Based on this, MOLLON et al [13] proposed a new two-dimensional failure mechanism with non-isometric logarithmic spirals, which is generated by a spatial discretization technique and can take the spatial variation of the internal friction angle into account, to calculate the upper bound value of the critical collapse pressure for a shield-driven tunnel. This presented kinematical approach was validated in comparison with the numerical simulation. Subsequently, on the basis of previous studies, MOLLON et al [14] further employed the spatial discretization technique to build a three-dimensional collapse mode, and the upper bound magnitudes of the collapse pressure were improved with this new mechanism by 25%.

In this work, on the basis of the active failure mechanism generated by the spatial discretization technique, the upper bound solutions of supporting pressure were derived with limit analysis method by considering the anisotropy and inhomogeneity of the internal friction angle as well as the cohesion simultaneously. Meanwhile, the parametric study was conducted to discuss the influence of relevant parameters on the upper bound solutions as well as optimal failure mechanism.

2 Anisotropy and inheterogeneity of geomaterials

2.1 Anisotropy

Through the experimental investigations, CASAGRANDE and CARILLO [15] found that shear strength changes with different directions of the failure surface, and the law of the cohesion changing with different directions is shown in Fig. 1.

The cohesion c_ξ in the direction of the maximum principle stress, which is at an angle of ξ from the vertical direction, can be expressed as

$$c_\xi = c_h + (c_v - c_h)\cos^2 \xi \quad (1)$$

where c_v is the vertical principle cohesion and its maximum principle stress is in the horizontal direction; c_h is the horizontal principle cohesion and its maximum principle stress is in the vertical direction. The magnitude of c_v and c_h can be obtained by geotechnical experiments.

LO's research has shown that the ratio of the horizontal cohesion c_h to the vertical cohesion c_v at any location remains approximately a constant [16]. Hence, he defined a coefficient $k=c_h/c_v$, which represents the anisotropy of the soils, for the case of isotropic soils with $k=1$. The Eq. (1) can be therefore written as

$$c_\xi = c_h\left(1+(1/k-1)\cos^2 \xi\right) \quad (2)$$

where k changes from 0.6 to 1.56 [16−18].

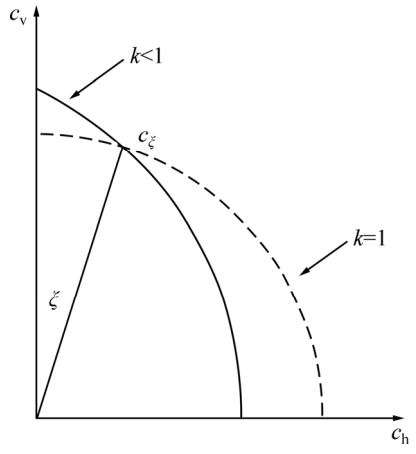

Fig. 1 Anisotropy of cohesion

2.2 Inhomogeneity

The cohesion increasing with the increase of depth z is the most common situation. In the study of foundation bearing capacity and slope stability, many scholars supposed some models for the inhomogeneity of the cohesion, as shown in Fig. 2. The inhomogeneity of the cohesion c follows the law in Fig. 2 and internal friction angle φ also follows such a similar variation.

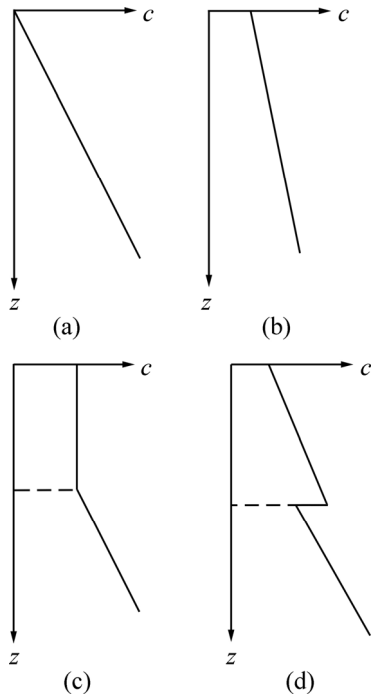

Fig. 2 Some models for inhomogeneity of cohesion

3 Active failure mechanism of tunnel face

Figure 3 presents the geometrical model for the problem in this work, where the point O' is the center of

the $A'B'$ and $A'B'$ represents the tunnel face, D is tunnel diameter and C is the buried depth. The ABE is the collapsing body; Point A and point B are the intersections between the collapsing body and the tunneling face respectively and Point F is the center of the AB. Theoretically, the collapse would be local failure if the soils exhibit inhomogeneity and anisotropy, so the collapsing body does not occur on the entire tunneling face but on the certain location in the middle of the tunnel face. Such a position is characterized by the parameter e and R, as illustrated in Fig. 3.

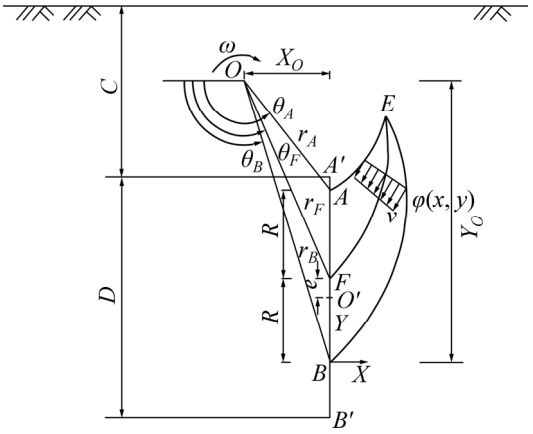

Fig. 3 Local collapsing mechanism

Point O is the rotational center of the collapsing body and ω is the rotational angular velocity. Other parameters, such as θ_A, θ_A, θ_F ,r_A, r_B and r_F, are shown in Fig. 3. In this work, the spatial discretization technique proposed by MOLLON et al [12−13] was used to generate the failure mechanism and the process is similar to that in Ref. [8].

Assuming that the coordinate of the rotational center O is (x_O, y_O), we can get following expressions:

$$r_A = \sqrt{x_O^2 + (y_O - 2R)^2} \tag{3}$$

$$r_B = \sqrt{x_O^2 + y_O^2} \tag{4}$$

$$\theta_A = \arctan(-\frac{x_O}{y_O - 2R}) \tag{5}$$

$$\theta_B = \arctan(-\frac{x_O}{y_O}) \tag{6}$$

$$\theta_E = \frac{1}{2}\left[\theta_A + \theta_B - \frac{\ln(\sin\theta_B / \sin\theta_A)}{\tan\varphi}\right] \tag{7}$$

The position of point O can be expressed as a function of r_F/R and θ_F:

$$\begin{cases} x_O = -R(\dfrac{r_F}{R}\cos\theta_F) \\ y_O = -R(\dfrac{r_F}{R}\sin\theta_F + 1) \end{cases} \tag{8}$$

Thus, the entire failure mechanism can be described by two dimensionless parameters which should meet the geometrical relationship:

$$\begin{cases} r_F / R > 1 \\ \pi/2 < \theta_F < \pi \end{cases} \tag{9}$$

4 Calculation of upper bound solution considering heterogeneity and anisotropy

4.1 Mode of heterogeneity and anisotropy

4.1.1 Heterogeneity of internal friction angle

Both the internal friction angle and cohesion in front of the tunneling face would change with the variation of depth.

In Fig. 4, φ_0 is the internal friction angle of point B', and the internal friction angle of any point $B_i(x_i, y_i)$ on the velocity discontinuity surface BE can be expressed as

$$\varphi_i = \varphi_0 - \rho_\varphi(y_i + D/2 + e - R) \tag{10}$$

where ρ_φ is the scale factor of the internal friction angle varying with the change of depth.

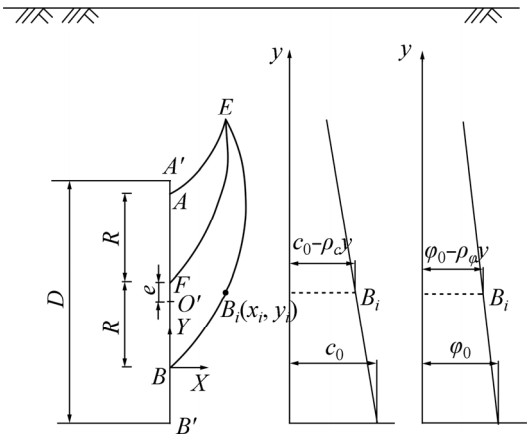

Fig. 4 Mode of heterogeneity

Define a dimensionless parameter k_φ as the inhomogeneity coefficient of the internal friction angle:

$$k_\varphi = \frac{\varphi_0 - 2D\rho_\varphi}{\varphi_0} \tag{11}$$

k_φ can reflect the varying situation that the internal friction angle changes with the depth: 1) $0<k_\varphi<1$ for the case that φ increases with the increase of depth, and the larger the k_φ, the greater the increase; 2) $k_\varphi=1$ for the case of homogenous soils; 3) $k_\varphi>1$ for the case that φ decreases with the increase of depth, and the smaller the k_φ, the greater the decrease.

4.1.2 Heterogeneity and anisotropy of cohesion

In Fig. 4, c_0 is the cohesion of point B', and the cohesion of any point $B_i(x_i, y_i)$ on the velocity discontinuity surface BE can be expressed as

$$c_i = c_0 - \rho_c(y_i + D/2 + e - R) \tag{12}$$

where ρ_c is the scale factor of the cohesion varying with the change of depth.

Define a dimensionless parameter k_c as the inhomogeneity coefficient of the cohesion:

$$k_c=\frac{c_0-2D\rho_c}{c_0} \tag{13}$$

k_c can reflect the varying situation that the cohesion changes with the depth: 1) $0<k_c<1$ for the case that c is positive to the depth, and the larger the k_c, the greater the increase; 2) $k_c=1$ for the case of homogenous soils; 3) $k_c>1$ for the case that c is negative to the depth, and the greater the k_c, the smaller the decrease.

The geometrical relationships of the anisotropic parameters are shown in Fig. 5. ψ is the angle between the velocity discontinuity surface and the maximum principal stress which acts on the velocity discontinuity surface. Corresponding research has proven that angle ψ is basically a constant regardless of the direction of the maximum principal stress. It is easy to obtain the expression of ξ from Fig. 5:

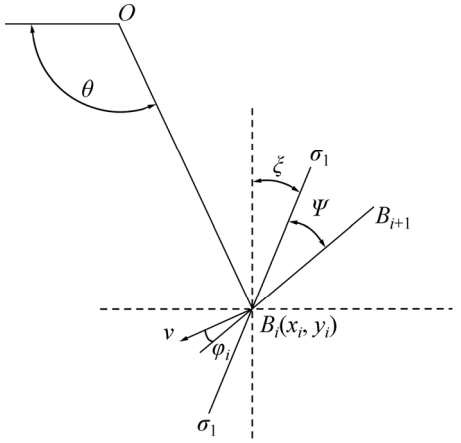

Fig. 5 Relationship of anisotropic cohesion

$$\xi=\pi-\theta_i-\varphi_i-\psi \tag{14}$$

Thus, Eq. (2) can be written as

$$c_\xi=c_h\left(1+(\frac{1}{k}-1)\cos^2(\pi-\theta_i-\varphi_i-\psi)\right) \tag{15}$$

where φ_i is the internal friction angle of point $B_i(x_i, y_i)$ and can be calculated based on Eq. (10), θ_i is the angle between the line OB_i and the initial direction, and it can be expressed by the following equation:

$$\theta_i=\pi-\arctan\frac{y_i-y_O}{x_i-x_O} \tag{16}$$

By substituting Eq. (12) into Eq. (15), the expression of the cohesion of point $B_i(x_i, y_i)$ results in

$$c_\xi=\left(c_0-\rho_c(y_i+D/2+e-R)\right)(1+(1/k-1)\cdot \cos^2(\pi-\theta_i-\varphi_i-\psi)) \tag{17}$$

4.2 Calculation of power of self-weight

In order to calculate the power rate generated by soil weight, the mechanism is subdivided into two main sections, as shown in Fig. 6.

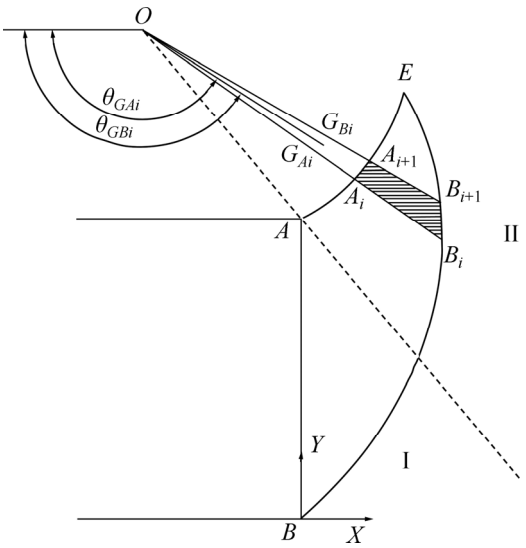

Fig. 6 Diagram used for calculation of power of unit weight

As shown in Fig. 6, the calculation of the rate of the weight of each triangle element AB_iB_{i+1} is first conducted separately, and then the work rate of the weight of part I can be obtained by adding the rate of the weight of all elements:

$$W_1=-\gamma\omega\sum_i S_iR_{Gi}\cos\theta_{Gi} \tag{18}$$

where S_i is the area of a triangle element AB_iB_{i+1} and it can be computed by the following expression:

$$S_i=\frac{1}{2}\delta\theta\sqrt{(x_i-x_A)^2+(y_i-y_A)^2}\cdot \sqrt{(x_{i+1}-x_A)^2+(y_{i+1}-y_A)^2} \tag{19}$$

(x_A, y_A) is the coordinate of point A,

$$\begin{cases}x_A=0\\ y_A=2R\end{cases} \tag{20}$$

G_i is the centre of gravity of triangle element AB_iB_{i+1} and the expression of its coordinate is

$$\begin{cases}x_{G_i}=\dfrac{x_A+x_{i+1}+x_i}{3}\\ y_{G_i}=\dfrac{y_A+y_{i+1}+y_i}{3}\end{cases} \tag{21}$$

R_{G_i} is the distance between the point O and the centre of gravity of triangle element AB_iB_{i+1}, and its expression is

$$R_{G_i}=\sqrt{(x_{G_i}-x_O)^2-(y_{G_i}-y_O)^2} \tag{22}$$

According to geometrical relationship, one can get

the expression of θ_{G_i}:

$$\theta_{G_i}=\pi-\arctan\frac{y_{G_i}-y_O}{x_{G_i}-x_O} \tag{23}$$

For the computation of the work rate of the weight of an element $A_iB_iB_{i+1}A_{i+1}$ in the Section II, it can be calculated by subtracting the power of the weight of the element OA_iA_{i+1} from the element OB_iB_{i+1}. Then, the work rate of the weight of Part II can be obtained by adding the work rate of the weight of all elements:

$$W_2=-\gamma\omega\sum_i(S_{B_i}R_{G_{Bi}}\cos\theta_{G_{Bi}}-S_{A_i}R_{G_{Ai}}\cos\theta_{G_{Ai}}) \tag{24}$$

where S_{B_i} is the area of triangle element OB_iB_{i+1}; S_{A_i} shows the area of triangle element OA_iA_{i+1}; $R_{G_{Bi}}$ represents the distance between the point O and the centre of gravity of triangle element OB_iB_{i+1}; $R_{G_{Ai}}$ indicates the distance between the point O and the centre of gravity of triangle element OA_iA_{i+1}; $\theta_{G_{Bi}}$ is the angle between the line OG_{Bi} and the initial direction; $\theta_{G_{Ai}}$ characterises the angle between the line OG_{Ai} and the initial direction. The calculation of these parameters is similar to Eqs. (23) and (24). Therefore, the power of gravity of the total failure mechanism is

$$W=W_1+W_2 \tag{25}$$

4.3 Calculation of work rate of supporting pressure

The supporting forces acting on the tunnel face are regarded as uniform loads and the power of the supporting forces can be computed by analytical method:

$$P_{\mathrm{f}}=\frac{1}{2}\sigma\omega r_B^2\left(\frac{\cos^2\theta_B}{\cos^2\theta_A}-1\right) \tag{26}$$

where r_B, θ_A and θ_B are given in Eqs. (4), (5) and (6).

4.4 Computation of power of energy dissipation

The energy dissipation only takes place on the velocity discontinuity surfaces due to assumption of the rigid rotation. The velocity discontinuity surfaces are generated by many successive segments, so the energy dissipation can be computed at each segment. The energy dissipation of the velocity discontinuity surface BE can be calculated by the following expression:

$$D_{BE}=c_{B_\xi}\omega\sum_{i=1}L_{B_i}R_{B_i}\cos\varphi_{B_i} \tag{27}$$

where L_{B_i} is the distance of B_iB_{i+1}:

$$L_{B_i}=\sqrt{(x_{i+1}-x_i)^2+(y_{i+1}-y_i)^2} \tag{28}$$

R_{B_i} is the distance between the point O and the midpoint of B_iB_{i+1}:

$$R_{B_i}=\sqrt{(\frac{x_{i+1}+x_i}{2}-x_O)^2-(\frac{y_{i+1}+y_i}{2}-y_O)^2} \tag{29}$$

φ_{B_i} is the internal friction angle at the midpoint of B_iB_{i+1}:

$$\varphi_{B_i}=\varphi_0-\rho_\varphi\left((y_{i+1}+y_i)/2+D/2+e-R\right) \tag{30}$$

c_{B_ξ} is the cohesion at the midpoint of B_iB_{i+1}:

$$c_{B_\xi}=(c_0-\rho_c((y_{i+1}+y_i)/2+D/2+e-R))\cdot(1+(1/k-1)\cos^2(\pi-\theta_i-\varphi_i-\psi)) \tag{31}$$

The energy dissipation of the velocity discontinuity surface AE can be calculated as

$$D_{AE}=c_{A_\xi}\omega\sum_{i=1}L_{A_i}R_{A_i}\cos\varphi_{A_i} \tag{32}$$

where the meanings of parameters L_{A_i}, R_{A_i}, φ_{A_i} and C_{A_ξ} are similar to those in Eqs. (28)−(31). Therefore, the energy dissipation of the total system is

$$D=D_{AE}+D_{BE} \tag{33}$$

4.5 Upper bound solutions of supporting forces

By equating the external power to the internal energy dissipation, the virtual work-rate equation can be expressed as

$$W-P_{\mathrm{f}}=D \tag{34}$$

Through solving Eq. (34), one can obtain the upper bound solutions of the supporting pressure as follows:

$$\sigma=-\left[\gamma\sum_i S_iR_{G_i}\cos\theta_{G_i}+\gamma\sum_i(S_{B_i}R_{G_{Bi}}\cos\theta_{G_{Bi}}-S_{A_i}R_{G_{Ai}}\cos\theta_{G_{Ai}})+c_{B_\xi}\sum_i L_{B_i}R_{B_i}\cos\varphi_{B_i}+c_{A_\xi}\omega\sum_i L_{A_i}R_{A_i}\cos\varphi_{A_i}\right]\Big/\frac{1}{2}r_B^2\left(\frac{\cos^2\theta_B}{\cos^2\theta_A}-1\right) \tag{35}$$

Therein, the supporting force is a function of r_F/R and θ_F.

5 Influence of heterogeneity and anisotropy on supporting forces

5.1 Influence of anisotropy of cohesion

The influence of the cohesion c on the supporting forces is discussed with relevant parameters corresponding to k_{c}=1.0, k_φ=1.0, c_0=10 kPa, γ=20 kg/m^3, D=12 m, C/D=2, R=6 m, e=0 m and $\delta\theta$=1°. The results are shown in Fig. 7.

It can be seen in Fig. 7 that the supporting forces increase with the increase of the cohesion anisotropy coefficient k. This is due to the fact that a bigger cohesion anisotropy coefficient k means a greater average cohesion c and the collapse is more difficult to happen even if the supporting forces are relatively smaller. Figure 8 presents the optimal failure mechanism with different cohesion anisotropy coefficient k. It is shown that the failure mechanism extends outward when

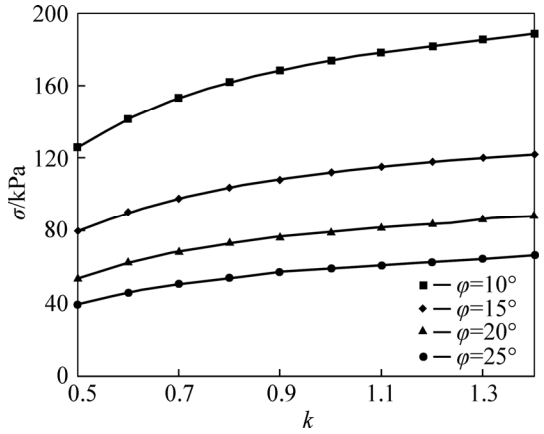

Fig. 7 Relationship between k and σ

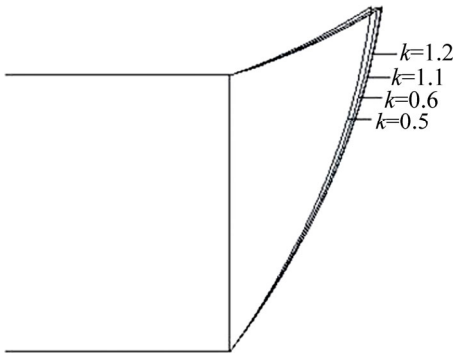

Fig. 8 Impact of k on shape of failure mechanism

the anisotropic coefficient k increases.

5.2 Influence of heterogeneity of cohesion

Figure 9 presents the σ values with different heterogeneity coefficient k_c of cohesion in the absence of the anisotropy of cohesion and the heterogeneity of internal friction angle when c_0=25 kPa, γ=20 kg/m^3, D=10 m, C/D=2, R=5 m, e=0 m and $\delta\theta$=1°.

As shown in Fig. 9, the supporting forces linearly decrease with increasing the value of heterogeneity coefficient k_c of cohesion, which means that the magnitude of cohesion has great influence on the supporting forces. This is because the larger k_c means the bigger cohesion and the better self-stability of the soils. According to analysis, it can be found that the failure mechanism is contracting inward with the increase of k_c but this trend is not very obvious.

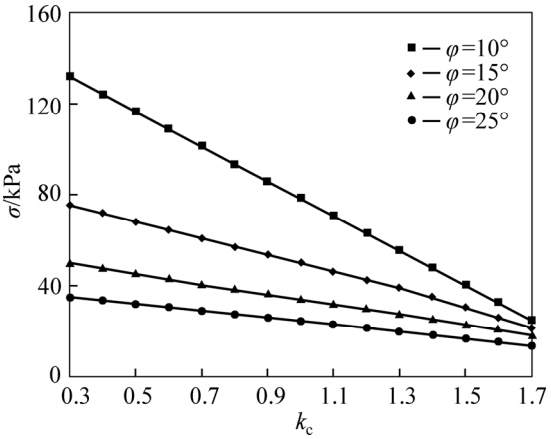

Fig. 9 Relationship between k_c and supporting forces

5.3 Influence of heterogeneity of internal friction angle

The change law of σ values with different heterogeneity coefficient k_φ of internal friction angle is obtained, as shown in Fig. 10, in the absence of the anisotropy and the heterogeneity of cohesion when c_0= 20 kPa, γ=20 kg/m^3, D=8 m, C/D=1, R=5 m, e=0 m and $\delta\theta$=1°. As illustrated in Fig. 10, the supporting forces are linearly negative to the value of k_φ, although the influence is not obvious. This is due to the interpretation that the larger the k_φ, the bigger the internal friction angle and the better the self-stability of the soils.

The optimal failure mechanisms with different k_φ are optimized, as illustrated in Fig. 11. It can be found that the failure mechanism contracts inwardly along with the increase of k_c, and this trend is relatively obvious compared with the precious conditions.

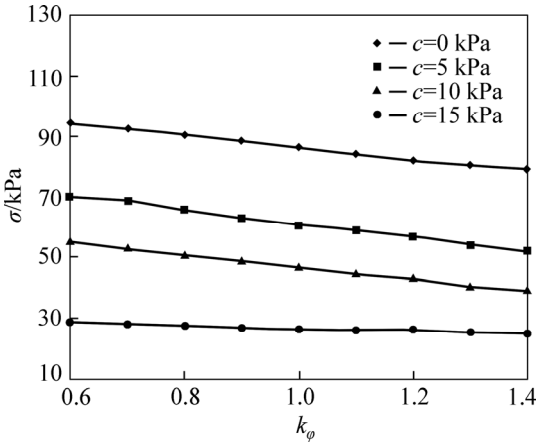

Fig. 10 Relationship between k_φ and supporting forces

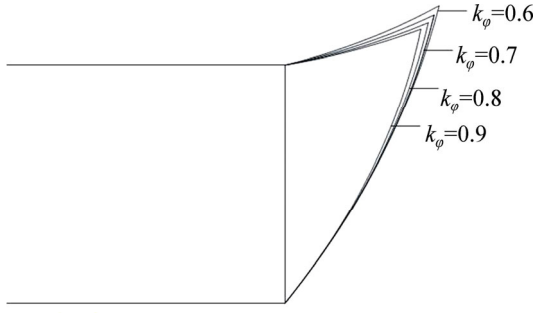

Fig. 11 Impact of k_φ on optimal failure mechanism

5.4 Influence of heterogeneity and anisotropy of cohesion

With the presence of anisotropy and heterogeneity of cohesion, the change law of the supporting forces is investigated when φ_0=25°, c_0=20 kPa, γ=20 kg/m^3, D= 10 m, C/D=2.0, R=5 m, e=0 m and $\delta\theta$=1°.

As shown in Fig. 12, the supporting forces increase with the decrease of k_c, but the change is very little. Besides, the supporting pressure decreases when k increases and this influence is more obvious than that of k_c, from which one can conclude that k has a larger impact on the supporting forces than k_c does.

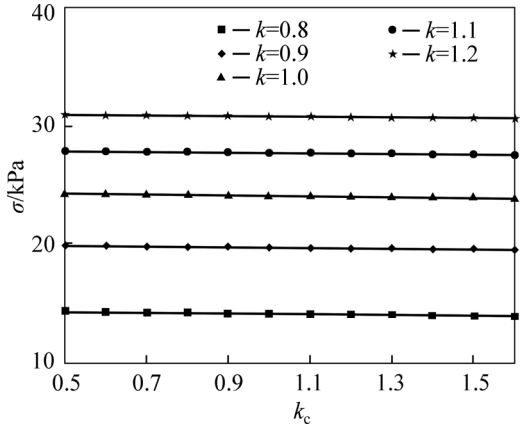

Fig. 12 Impact of k_c and k on supporting forces

5.5 Influence of heterogeneity of internal friction angle and anisotropy of cohesion

Under the condition of the anisotropy of cohesion and the heterogeneity of internal friction angle, the change rule of σ values is plotted in Fig. 13 when φ_0=20°, c_0=10 kPa, γ=20 kg/m^3, D=10 m, C/D=2.0, R=5 m, e=0 m and $\delta\theta$=1°. It can be easily found from Fig. 13 that, the supporting forces are positive to the value of k, but the trend grows slowly. However, the effect of k_φ shows an opposite change pattern, i.e., the supporting pressure increases with the decreasing magnitude of k_φ, which indicates that both k and k_φ have an important influence on the supporting forces.

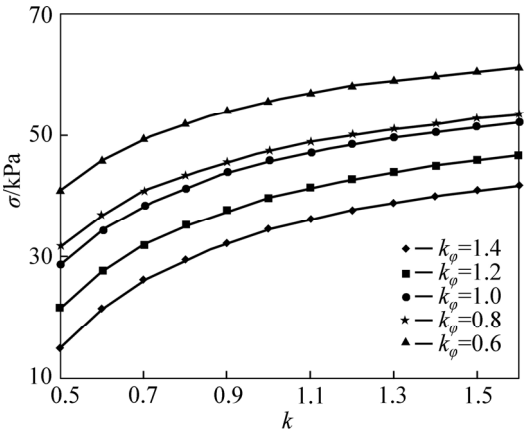

Fig. 13 Influence of k_φ and k on supporting forces

5.6 Influence of heterogeneity of internal friction angle and cohesion

Considering the heterogeneity of cohesion and internal friction angle, the change pattern of σ values is illustrated in Fig. 14 when φ_0=25°, c_0=20 kPa, γ=20 kg/m^3, D=10 m, C/D=2.0, R=5 m, e=0 m and $\delta\theta$=1°.

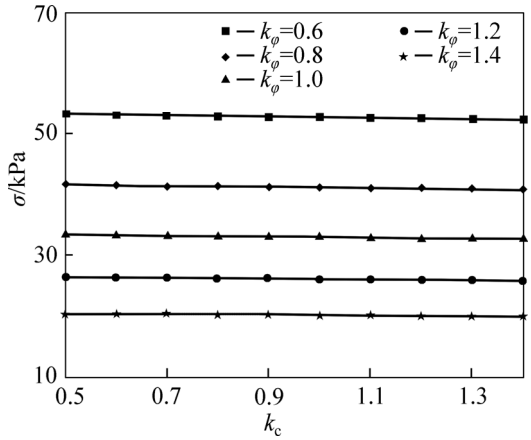

Fig. 14 Influence of k_φ and k_c on supporting forces

Figure 14 shows that the supporting forces have a positive relationship with the value of k_c, but the decreasing trend is very small. Besides, the supporting forces decrease with the increase of k_φ.

6 Conclusions

1) Without taking into account the heterogeneity of cohesion and internal friction angle, the supporting pressure tends to increase, and the failure mechanism extends outward with increasing the value of cohesion anisotropy coefficient k, although it changes slowly. However, the collapse pressure shows an opposite trend and the failure mechanism extends inward with the increase of heterogeneity coefficient k_c of cohesion and it attenuates linearly and greatly in the absence of anisotropy of cohesion and heterogeneity of internal friction angle. Moreover, with the increase of heterogeneity coefficient k_φ of internal friction angle, the supporting pressure decreases linearly and the collapse mechanism shrinks inward without considering anisotropy and the heterogeneity of cohesion.

2) The effect of cohesion anisotropy coefficient k on supporting pressure is far more significant than that of heterogeneity coefficient k_c due to the amplitude of variation, while both cohesion anisotropy coefficient k and heterogeneity coefficient k_φ have an obvious influence on the collapse pressure of excavation face, although the amplification varies in diverse conditions.

References

[1] SAADA Z, MAGHOUS S, GARNIER D. Pseudo-static analysis of tunnel face stability using the generalized Hoek-Brown strength criterion [J]. International Journal for Numerical and Analytical Methods in Geomechanics, 2013, 37(18): 3194−3212.

[2] LI Y, EMERIAUL F, KASTNER R, ZHANG Z X. Stability analysis of large slurry shield-driven tunnel in soft clay [J]. Tunnelling and Underground Space Technology, 2009, 24: 472−481.

[3] SENENT S, MOLLON G, JIMENEZ R. Tunnel face stability in heavily fractured rock masses that follow the Hoek-Brown failure criterion [J]. International Journal of Rock Mechanics and Mining Sciences, 2013, 60(1): 440−451.

[4] MAO N, AL-BITTAR T, SOUBRA A H. Probabilistic analysis and design of strip foundations resting on rocks obeying Hoek-Brown failure criterion [J]. International Journal of Rock Mechanics and Mining Sciences, 2012, 49: 45−58.

[5] AZAMI A, PIETRUSZCZAK S, GUO P. Bearing capacity of shallow foundations in transversely isotropic granular media [J]. International Journal for Numerical and Analytical Methods in Geomechanics, 2010, 34: 771−793.

[6] SAADA Z, MAGHOUS S, GARNIER D. Pseudo-static analysis of tunnel face stability using the generalized Hoek-Brown strength criterion [J]. International Journal for Numerical and Analytical Methods in Geomechanics, 2013, 37(8): 3194−3212.

[7] MICHALOWSKI R, NADUKURU S. Three-dimensional limit analysis of slopes with pore pressure [J]. Journal of Geotechnical and Geoenvironmental Engineering, 2012, 139(9): 1604−1610.

[8] QIN C B, SUN Z B, LIANG Q. Limit analysis of roof collapse in tunnels under seepage forces condition with three-dimensional failure mechanism [J]. Journal of Central South University, 2013, 20(8): 2314−2322.

[9] SUN Zhi-bin, ZHANG Dao-bing. Back analysis for soil slope based on measuring inclination data [J]. Journal of Central South University, 2012, 19(11): 3291−3297.

[10] SUN Zhi-bin, LI Qiao. Back analysis of general slope under earthquake forces using upper bound theorem [J]. Journal of Central South University, 2013, 20(11): 3274−3281.

[11] SUBRIN D, WONG H. Tunnel face stability in frictional material: A new 3D failure mechanism [J]. Computes Mechanique, 2012, 330(7): 513−519.

[12] MOLLON G, DIAS D, SOUBRA A H. Probabilistic analysis and design of circular tunnels against face stability [J]. International Journal of Geomechanics, 2009, 9(6): 237−249.

[13] MOLLON G, DIAS D, SOUBRA A H. Rotational failure mechanisms for the face stability analysis of tunnels driven by a pressurized shield [J]. International Journal for Numerical and Analytical Methods in Geomechanics, 2011, 35(12): 1363−1388.

[14] MOLLON G, PHOON K K, DIAS D, SOUBRA A H. Validation of a new 2D failure mechanism for the stability analysis of a pressurized tunnel face in a spatially varying sand [J]. Journal of Engineering Mechanics, 2011(1): 8−20.

[15] CASAGRANDE A, CARILLO N. Shear failure of anisotropic materials [J]. Journal of Boston Society of Civil Engineers, 1944, 31(4): 74−81.

[16] LO K Y. Stability of slopes in anisotropic soils [J]. Journal of the Soil Mechanics and Foundations Division, 1965, 91(4): 85−106.

[17] DAVIS E H, BOOKER J R. The effect of increasing strength with depth on the bearing capacity of clays [J]. Geotechnique, 1973, 23(4): 551−563.

[18] LEE K M, ROWE R K. Effects of undrained strength anisotropy on surface subsidence induced by the construction of shallow tunnels [J]. Canadian Geotechnical Journal, 1986, 26(3): 279−291.

(Edited by YANG Bing)